Capturing self-propelled particles in a moving microwedge

A. Kaiser,[1,*] K. Popowa,[1] H. H. Wensink,[2] and H. Löwen[1]

[1]*Institut für Theoretische Physik II: Weiche Materie, Heinrich-Heine-Universität Düsseldorf, Universitätsstraße 1, D-40225 Düsseldorf, Germany*

[2]*Laboratoire de Physique des Solides, Université Paris-Sud and CNRS, Bâtiment 510, 91405 Orsay Cedex, France*

(Received 28 June 2013; published 21 August 2013)

Catching fish with a fishing net is typically done either by dragging a fishing net through quiescent water or by placing a stationary basket trap into a stream. We transfer these general concepts to micron-sized self-motile particles moving in a solvent at low Reynolds number and study their collective trapping behavior by means of computer simulations of a two-dimensional system of self-propelled rods. A chevron-shaped obstacle is dragged through the active suspension with a constant speed v and acts as a trapping "net." Three trapping states can be identified corresponding to no trapping, partial trapping, and complete trapping and their relative stability is studied as a function of the apex angle of the wedge, the swimmer density, and the drag speed v. When the net is dragged along the inner wedge, complete trapping is facilitated and a partially trapped state changes into a complete trapping state if the drag speed exceeds a certain value. Reversing the drag direction leads to a reentrant transition from no trapping to complete trapping and then back to no trapping upon increasing the drag speed along the outer wedge contour. The transition to complete trapping is marked by a templated self-assembly of rods forming polar smectic structures anchored onto the inner contour of the wedge. Our predictions can be verified in experiments of artificial or microbial swimmers confined in microfluidic trapping devices.

DOI: 10.1103/PhysRevE.88.022311 PACS number(s): 82.70.Dd, 61.20.Lc, 61.30.Pq, 87.15.A−

I. INTRODUCTION

With an appropriate use of a fishing net, many fish can be simultaneously caught in an efficient way. There are two different strategies to catch fish using, e.g., a cone-shaped net; either the net can be dragged through quiescent water or a stationary trap (a so-called fyke) can be placed in running water, forcing the fish to swim into the fyke. While the general methods for trapping macroscopic swimming organisms (fish) have been known since ancient times [1], the corresponding problem in the microscale has been scarcely explored thus far due to the general difficulty in controlling and designing processes in systems of micron-sized objects. There are many realizations of microscopic swimmers [2–5], including autonomously navigating microbes [6–16] and human-made artificial swimmers [17–30]. For many applications it is of key importance to trap collections of these active particles into a moving trap. A first application is to transport ensembles of swimmers to a given destination like a cargo. This situation differs from the more commonly considered case in which the swimmer itself transports an inert cargo [31–35]. It is obvious that, in the former situation, one, first, has to catch the particles in an efficient and controlled way before they can be transferred to the specific destination via a moving trap. A second application could be to efficiently remove "dangerous" toxic particles in order to clean the environment [36,37]. Moreover, the motion of the trap is expected to play a crucial role in optimizing the removal of contaminating mesogens.

Apart from the different length scale, it is important to note that another basic difference between macroscopic fish and microbes is their Reynolds number Re, which characterizes the ratio of inertial to viscous forces associated with swimming. While fish typically swim at a Reynolds number of several hundred, microswimmers typically operate at very low Reynolds numbers, $\mathrm{Re} \ll 1$.

In this paper, we transfer the ideas of catching fish in a net to micron-sized self-motile particles propagating through a solvent at a low Reynolds number. We use computer simulations of a two-dimensional system of self-propelled rods and drag a chevron-shaped obstacle with a constant speed v through the embedding active fluid. As revealed by a simple Galilean transformation, this setup is equivalent to a static trap in a flowing solvent. Our simulations complement earlier studies for a static trap [38] where a wedge was found to optimize the catching efficiency. Here we focus on the effect of a nonzero drag speed. At fixed swimmer density and varied drag velocity v and apex angle of the trap, there are three emerging states corresponding to no trapping, partial trapping, and complete trapping. While in the no-trapping state no particles remain in the trap over time, in the complete trapping state all swimmers are permanently caught in the microwedge after a certain amount of time. Finally, partial trapping refers to a state where only a fraction of the particles are permanently trapped. Obviously, the dream of any fishermen and the most desirable situation in many applications is the complete-trapping state, where no freely moving particles are left.

We solve the single-rod case analytically and present the trapping state diagram in the plane spanned by the opening angle α of the microwedge ($0 < \alpha \leqslant \pi$) and the trap velocity v (normalized by the swimmer velocity v_0). The drag direction is along the symmetry axis of the wedge and we define a positive drag speed if its drag is along the inner part of the wedge. As a result, if the net is dragged into the positive direction, trapping is facilitated. Counterintuitively, however, for a negative drag velocity, a situation of no trapping can change into a trapped one, which we attribute to polar ordering of the swimmer along the wedge symmetry axis. Clearly, when the (negative) trap

*kaiser@thphy.uni-duesseldorf.de

velocity exceeds the swimmer velocity ($v/v_0 < -1$), trapping is no longer possible as the trap overtakes the swimmer, which leads to a reentrant effect for increasing negative velocity: for intermediate opening angles α, we observe the state sequence of no trapping, complete trapping, and no trapping. For finite trap density we employ computer simulations [38–40] and confirm the trends of single-particle trapping. For high-enough positive drag speed, a partial trapped situation will change into a complete trapped situation. In the converse case of a negative trap velocity, the reentrance effect is amplified by a collective polar ordering in the trap. This is a typical example of self-assembly of self-propelled colloidal rods [41] directed by the moving microwedge. Previous studies analyzing the rectification effect of a wall of funnels by experiments [42,43], theory [44], and simulation [45–48] have utilized similar chevron-shaped boundaries but have never focused on trapping.

Apart from their relevance for applications, our predictions can be verified in experiments on rodlike microbes and self-propelled colloids and granulates [42,49–52]. Typically, the system is moving on a two-dimensional substrate or can be subject to a strong two-dimensional confinement [53]. A chevronlike trap can be prepared by lithographic techniques [22,23,54,55] and it can be dragged at will using optical tweezers [56,57]. Therefore, an experimental realization of our model is conceivable. We further anticipate that the same effects occur also in three dimensions where the corresponding generalization of the wedgelike trap is a hollow cone, similar in spirit to a real fishing net.

This paper is organized as follows: in Sec. II we introduce the model and explain the simulation method. Section III is devoted to the case of a single self-propelled rod. We will give a theoretical prediction of the trapping state diagram along with numerical results. In Sec. IV, we investigate the trapping states for many particles and all three main control parameters. In particular, we fix each time one of these, vary the others, and obtain a full trapping state diagram which can be explained by the effects already showing up for the single-particle case. Finally, we conclude in Sec. V.

II. MODEL

The aim is to formulate a minimal collision-based model for self-propagating rod-shaped particles that is capable of capturing the generic features of interacting swimmers at intermediate to high particle density and their collective response to mobile confining boundaries. Following earlier studies [38,58], our system consists of N rigid rods of length ℓ, each moving in the overdamped limit with a propagation velocity v_0 arising from a formal force F_0 fixed along the longitudinal rod axis $\hat{\mathbf{u}}$ [39,58]. This does not contradict the basic fact that a swimmer is force free. The actual position of the αth rod ($\alpha = 1, \ldots, N$) is described by a center-of-mass position vector $\mathbf{r}_\alpha$ and a unit orientational vector $\hat{\mathbf{u}}_\alpha = (\cos\varphi_\alpha, \sin\varphi_\alpha)$.

Due to solvent friction, the particles move in the overdamped low-Reynolds-number regime, while interacting with the other particles and the boundary by steric forces only [39]. The latter are implemented by discretizing each rod into a linear array of n equidistant spherical segments and imposing a repulsive Yukawa potential between the segments of each pair [59,60]. The total pair potential between rods $\{\alpha,\beta\}$ with orientational unit vectors $\{\hat{\mathbf{u}}_\alpha,\hat{\mathbf{u}}_\beta\}$ and center-of-mass distance $\Delta\mathbf{r}_{\alpha\beta} = \mathbf{r}_\alpha - \mathbf{r}_\beta$ is then given by

$$U_{\alpha\beta} = U_0 \sum_{i=1}^{n}\sum_{j=1}^{n} \frac{\exp\left[-r_{ij}^{\alpha\beta}/\lambda\right]}{r_{ij}^{\alpha\beta}}, \tag{1}$$

where $U_0 > 0$ defines the amplitude, λ the screening length, and $r_{ij}^{\alpha\beta} = |\Delta\mathbf{r}_{\alpha\beta} + (l_i\hat{\mathbf{u}}_\alpha - l_j\hat{\mathbf{u}}_\beta)|$ the distance between segment i of rod α and j of rod β ($\alpha \neq \beta$) with $l_i = d(i-1)$, $i \in [1,n]$ denoting the segment position along the main rod axis. The number of rod segments n is chosen such that the intrarod segment distance $d = \ell/[(n+1)(n-1)]^{1/2} \leqslant \lambda$ and rod overlaps are prevented. A trap is introduced as a boundary with a prescribed shape and contour length ℓ_T and is dragged with a velocity v through the system. Particle-trap interactions are implemented by discretizing the trap boundary into $n_T = \lfloor \ell_T/d \rceil$ equidistant segments each interacting with the rod segments via the same Yukawa potential, resulting in the pair potential

$$U_{\alpha T} = U_0 \sum_{i=1}^{n}\sum_{k=1}^{n_T} \frac{\exp\left[-r_{ik}^{\alpha T}/\lambda\right]}{r_{ik}^{\alpha T}}. \tag{2}$$

Here $r_{ik}^{\alpha T}$ denotes the distance between segment i of rod α and segment k of the trap. The net is dragged with imposed velocity $\mathbf{v} = v\mathbf{x}$ along the symmetry axis of the wedge according to

$$\mathbf{r}_k = \mathbf{v}t, \tag{3}$$

where $\mathbf{r}_k$ denotes the position of the kth segment of the trap. Mutual self-propelled rod collisions generate apolar nematic alignment which stimulates swarm formation at finite concentrations [52]. The wedge boundary mimics a hard wall and imparts 2D planar order with rods pointing favorably perpendicular to the local wall normal.

The microscopic equations of motion for the center-of-mass position $\mathbf{r}_\alpha(t)$ and orientation $\hat{\mathbf{u}}_\alpha(t) = (\cos\varphi_\alpha(t), \sin\varphi_\alpha(t))$ of the self-propelled particles emerge from a balance of the forces and torques acting on each rod α and are similar as described in Ref. [58],

$$\mathbf{f}_\mathcal{T} \cdot \partial_t \mathbf{r}_\alpha = -\nabla_{\mathbf{r}_\alpha} U + F_0\hat{\mathbf{u}}_\alpha, \tag{4}$$

$$\mathbf{f}_\mathcal{R} \cdot \partial_t \hat{\mathbf{u}}_\alpha = -\nabla_{\hat{\mathbf{u}}_\alpha} U, \tag{5}$$

in terms of the total potential energy $U = (1/2)\sum_{\alpha,\beta(\alpha\neq\beta)} U_{\alpha\beta} + \sum_{\alpha,T} U_{\alpha T}$ with $U_{\alpha T}$ the potential energy of rod α with the trap and $\nabla_{\hat{\mathbf{u}}_\alpha}$ denotes the gradient on a unit circle. The one-body translational and rotational friction tensors $\mathbf{f}_\mathcal{T}$ and $\mathbf{f}_\mathcal{R}$ can be decomposed into parallel $f_\parallel$, perpendicular $f_\perp$, and rotational $f_\mathcal{R}$ contributions,

$$\mathbf{f}_\mathcal{T} = f_0\,[f_\parallel\hat{\mathbf{u}}_\alpha\hat{\mathbf{u}}_\alpha + f_\perp(\mathbf{I} - \hat{\mathbf{u}}_\alpha\hat{\mathbf{u}}_\alpha)], \tag{6}$$

$$\mathbf{f}_\mathcal{R} = f_0\, f_\mathcal{R}\mathbf{I}. \tag{7}$$

Hereby $\mathbf{I}$ is the 2D unit tensor and f_0 is a Stokesian friction coefficient. The dimensionless geometric factors $\{f_\parallel, f_\perp, f_\mathcal{R}\}$ depend solely on the aspect ratio $a = \ell/\lambda$, and we adopt the

standard expressions for rodlike macromolecules, as given in Ref. [61],

$$f_{||} = 2\pi(\ln a - 0.207 + 0.980a^{-1} - 0.133a^{-2})^{-1},$$
$$f_{\perp} = 4\pi(\ln a + 0.839 + 0.185a^{-1} + 0.233a^{-2})^{-1}, \quad (8)$$
$$f_{\mathcal{R}} = \frac{\pi a^2}{3}(\ln a - 0.662 + 0.917a^{-1} - 0.050a^{-2})^{-1}.$$

Equation (5) neglects thermal or intrinsic Brownian noise [62], which is acceptable at intermediate to high concentrations when particle collision dominate the dynamics [53]. Despite its minimal nature, the self-propelled rod model provides a remarkably accurate description of the velocity statistics and microstructure of dense active matter [53].

It is important to note that our system is strictly equivalent to a quiescent net where the swimmers all experience their propagation velocity $\mathbf{v}_0$ together with an added velocity $-\mathbf{v}$. This can easily be demonstated by transforming the equation of translational motion Eq. (4) in terms of reduced difference coordinates $\widetilde{\mathbf{r}}_\alpha = \mathbf{r}_\alpha - \mathbf{v}t$, i.e., by applying a *Galilean transformation* [63] so

$$\partial_t \widetilde{\mathbf{r}}_\alpha = (v_0\hat{\mathbf{u}}_\alpha - \mathbf{v}) - \mathbf{f}_T^{-1} \cdot \nabla_{\widetilde{\mathbf{r}}_\alpha} U. \quad (9)$$

The typical self-propulsion speed of a free single self-propelled rod

$$v_0 = \frac{F_0}{f_0 f_{||}} \quad (10)$$

defines the time interval

$$\tau = \frac{\ell}{v_0} \quad (11)$$

a rod needs to swim a distance comparable to its size. In the following, distances are measured in units of ℓ and energy in units of $F_0\ell$.

We simulate self-propelled rods with aspect ratio $a = 10$, using $n = 11$ segments, in a square simulation box with area A and periodic boundary conditions in both Cartesian directions. A particle packing fraction is defined as $\phi = N\sigma/A$ with $\sigma = \lambda(\ell - \lambda) + \lambda^2\pi/4$ the effective area of a single rod. In the bulk density range $\phi < 0.2$ the self-propelled rods spontaneously form flocks with strong spatial density fluctuations [64]. We subject the self-propelled rods to a mobile chevron boundary with contour length $\ell_T = 20\ell$ and variable apex angle $0^\circ < \alpha < 180^\circ$, leading to an occupied trap area $A_0 = (\ell_T^2/8)\sin\alpha/2$, which is dragged with velocity v (see Fig. 1). In the macroscopic limit, the system can be interpreted as a reservoir of microswimmers exposed to an equidistant array of mutually independent wedges. A reduced trap density is defined by $\phi_T = (\ell_T^2/8A)$ which fixes the number of rods via $N = (\ell_T^2/8\sigma)(\phi/\phi_T)$. We constrain $\phi_T = 0.031 < 0.1$ in order to guarantee the microwedges to be completely independent of each other within the typical range of bulk rod packing fractions $0 < \phi < 0.1$ considered here. The latter density is one of our main steering parameters. There are also the drag velocity which is in the range of $-1.2v_0 < v < 8v_0$ and the apex angle α of the microwedge.

Initial configurations are generated from a rectangular lattice of aligned rods with $\hat{\mathbf{u}}$ pointing randomly up or down. The rods are randomly displaced from the initial lattice such that the starting configuration bears already some randomness.

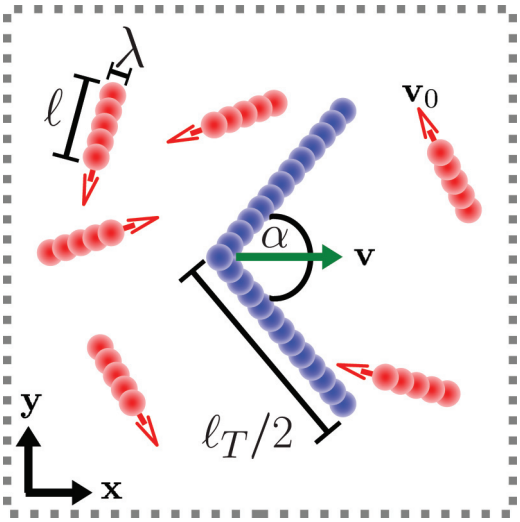

FIG. 1. (Color online) Sketch of the system of self-propelled rods with aspect ratio $a = \ell/\lambda$ and a self-motile velocity $\mathbf{v}_0$ directed along the main axis $\hat{\mathbf{u}}$ [red (light gray) arrows] of each rod at bulk density ϕ. The single Yukawa segments are shown as red spheres. A mobile wedge [indicated by blue (dark) spheres] with contour length ℓ_T and an apex angle α is dragged with a constant velocity $\mathbf{v}$ [green (filled gray) arrow]. Periodic boundary conditions in both Cartesian directions are indicated by dotted lines.

The segments of the microwedge are successively placed in the system to avoid overlapping rods. We simulate the whole system for a time of at least $t_s = 15\,000\tau$.

III. TRAPPING A SINGLE SWIMMER IN A MOBILE MICROWEDGE

We first focus on a single swimmer for which analytical results can be obtained which we test against our computer simulations. In Fig. 2(a), simulation results and analytical formulas for the trapping state diagram are combined. The main control parameters we vary are the reduced trap drag velocity v/v_0 and the apex angle α. The trapping scenario of a single swimmer is generic and is independent of the contour length of the net, as long as $\ell_T \gg \ell$, and the aspect ratio of the rod-shaped swimmer. In the simulation, a particle is considered to be trapped if it remains inside the wedge for at least $t^* = 10^3\tau$.

Let us, first, discuss some limiting cases which are all intuitive: For strongly negative drag velocities, $v/v_0 < -1$, the swimmer is slower than the microwedge and therefore can never get trapped for any opening angle α. Conversely, for $v/v_0 > -1$ and very small opening angles, once a rod enters the moving net it is faster than the net and therefore will approach to the kink of the wedge, where it remains because it cannot escape by turning around. Hence, there is a trapping state for $v/v_0 > -1$ and small opening angles. Complementarily, for $v/v_0 > -1$ and very large opening angles ($\alpha \approx \pi$), if the rod enters the microwedge, it will just slide along the wall of the wedge and will then pass over the slight kink of the wedge such that the rod leaves the trap again. Consequently, the rod does not permanently reside in the wedge and, thus, attains a no-trapping state.

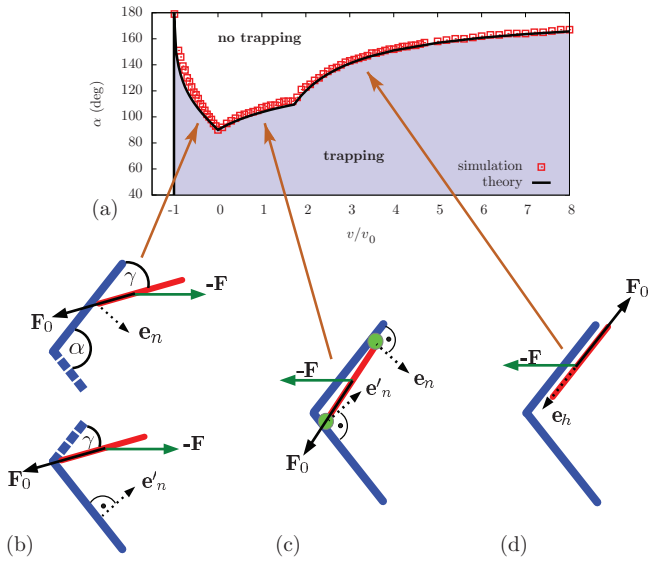

FIG. 2. (Color online) (a) Trapping state diagram for a single self-propelled rod in the plane of reduced drag velocities v/v_0 and net apex angles α. The shaded region marks the trapping regime. The dots represent simulation results for the trapping-no trapping boundary while the solid line contains the analytical predictions. Different trapping mechanisms are sketched in (b)–(d). For more details, see text. Points of contact of the swimmer and the microwedge are highlighted by light green (light gray) circles.

As shown in Fig. 2(a), the intermediate transition opening angle which separates the trapping from the no-trapping regime is a marked function of the reduced trap velocity which exhibits some cusps. The cusps occur at $v/v_0 = -1$, $v/v_0 = 0$, and $v/v_0 = \sqrt{3}$ and clearly distinguish four different situations which we now discuss quantitatively step by step. We use the frame of the resting net for this discussion and introduce forces instead of velocities. Clearly forces are proportional to velocities. In the microwedge system, the rod center experiences a force $\mathbf{F_0} \propto \mathbf{v}_0$ governing its self-propulsion plus another force $-\mathbf{F} \propto -\mathbf{v}$ arising from the resting rod frame. Third, the wall possibly exerts at contact a force $\mathbf{F}_N$ onto the rod which is always normal to the wall.

As already stated above, for strongly negative drag velocities, $v/v_0 < -1$, a swimmer moves slower than the microwedge and therefore can never get trapped. For $-1 < v/v_0 < 0$, it is expected that single rods are still spilled out by the net, but the opposite behavior is true: trapping becomes more efficient if the drag speed approaches the swimmer speed $v/v_0 \to -1^+$ from above. This counterintuitive behavior can be understood as sketched in Fig. 2(b). If a rod enters the trap and hits a wall (see upper sketch of Fig. 2(b) and Ref. [65]), it will orient at an angle γ. This angle is determined by the condition that the projection of $\mathbf{F_0} - \mathbf{F}$ onto the wall normal has to vanish, $(\mathbf{F}_0 - \mathbf{F}) \cdot \mathbf{e}_n = 0$, with the wall normal vector $\mathbf{e}_n = (\sin\alpha/2, -\cos\alpha/2)$. This leads to $\gamma = \arcsin(v/v_0)$. With this orientation, the rod will slide along the wall inside the corner until it touches the lower wedge wall [see lower sketch of Fig. 2(b)]. The threshold condition whether the rod slides further outside the wedge along the lower wall is finally given by requiring that the normal projection along the lower wall normal $\mathbf{e}'_n = (\sin\alpha/2, \cos\alpha/2)$ vanishes, i.e., $(\mathbf{F}_0 - \mathbf{F}) \cdot \mathbf{e}'_n = 0$. This all leads to the threshold condition

$$\alpha = \frac{\pi}{2} - 2\left[\arcsin\left(\frac{v}{\sqrt{2}v_0}\right) - \arcsin\left(\frac{v}{v_0}\right)\right], \qquad (12)$$

which is plotted as a solid line in Fig. 2(a). This implies that a trap moving into the negative direction orients the rods along the wedge symmetry axis and, thus, keeps them inside, thereby enhancing the trapping efficiency.

In the case of positive drag velocities, two different trapping mechanisms can occur. The first mechanism is shown in Fig. 2(c) and Ref. [65]. Here the swimmer enters into the wedge and is stuck close to the wedge cusp with two contact points, one at the higher and another at the lower wall. This hinders the rod in rotating further such that it gets immobilized. The contact points are indicated in Fig. 2(c). In this situation, the rod experiences four different forces, two arising simultaneously from the wall normals plus $\mathbf{F_0} - \mathbf{F}$. The normal wall forces are unknown but determined by the joint conditions of the vanishing total force and the torque acting on the rod center which characterize the transition from no trapping to trapping. Hence, these conditions are $\mathbf{F}_0 - \mathbf{F} + \mathbf{F}_n + \mathbf{F}'_n = 0$ and $F_n \mathbf{e}_h \times \mathbf{e}'_n + F'_n \mathbf{e}_h \times \mathbf{e}_n = 0$. Eliminating the unknown normal forces, we obtain the threshold criterion

$$\frac{v}{v_0} = -\cos\left(\frac{\alpha}{2}\right) + \frac{\sin^4(\alpha/2)}{\cos^3(\alpha/2)}. \qquad (13)$$

The second mechanism is shown in Fig. 2(d) (see also Ref. [65]) and refers to a situation where an aligned rod intends to leave the trap, for example, when it was able to turn in the kink. If the projection of $-\mathbf{F}$ tangential to the wall exceeds the self-propulsion, the moving microwedge surpasses the rod and keeps it caught. The condition for the threshold for this second mechanism is, therefore $\mathbf{F} \cdot \mathbf{e}_h = F_0$ for $\mathbf{e}_h = (-\cos\alpha/2, -\sin\alpha/2)$, which yields

$$\cos\left(\frac{\alpha}{2}\right) = \frac{1}{v/v_0}. \qquad (14)$$

As can be shown easily, this second mechanism surpasses the former mechanism for dragging velocities $v/v_0 > \sqrt{3}$.

Summarizing, a single self-propelled particle can always be trapped for $v > -v_0$ and $\alpha < 90^\circ$. For apex angles larger than 90° and increasing trap velocities, the following sequence of states is found: no trapping, trapping, no trapping, and trapping. This clearly demonstrates the nontrivial interplay between wedge geometry and orientational coupling to the rod. Moreover, we find for positive drag velocities two different mechanisms which hold the particles inside the microwedge. Finally, the good agreement of the threshold lines between analytical theory and simulations shows that the segment model used in this paper reproduces well the purely geometric conditions of steeply repulsive interactions.

IV. COLLECTIVE TRAPPING

A. Static microwedge

Let us, first, briefly recapitulate previous results [38] for a static trap ($v = 0$). The trapping state diagram now drawn in the parameter space spanned by the net apex angle α and reduced rod packing fraction ϕ_R at fixed net densities is shown in Fig. 3, including characteristic snapshots.

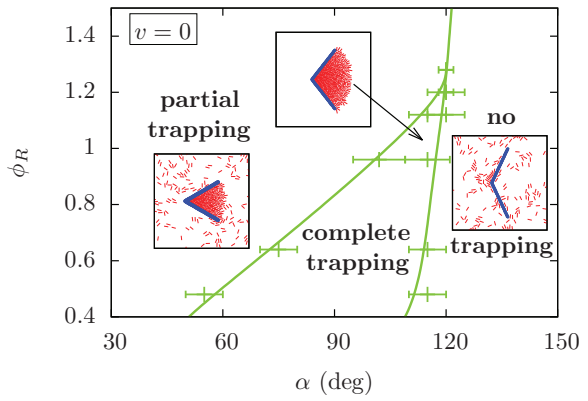

FIG. 3. (Color online) Trapping state diagram in the case of a static trap $v = 0$ denoting three different states for varying apex angles and a reduced self-propelled rod packing fraction. All occurring trapping states are visualized by use of characteristic snapshots using central sections of the simulation box.

Following earlier work [38], we consider a rod α trapped if its velocity $v_\alpha = |\mathbf{v}_\alpha| < 0.1 v_0$ for a time interval $t^* = 25\tau$. In contrast to the single-particle case we now have to distinguish between two different kinds of trapped states. These are characterized by the fraction of trapped particles x_T which acts as some kind of order parameter for the different states. Either no particle is trapped, $x_T = 0$ (no trapping), or all particles are trapped, $x_T = 1$ (complete trapping), or just a fraction of all particles in the system can be captured by the wedge, $0 < x_T < 1$. This new state will be referred to as partial trapping.

All trapping states can be found in the state diagram for a static microwedge; see Fig. 3. Evidently, in the case of small apex angles there is only partial trapping since the area of the wedge is too small to accommodate all particles.

Larger apex angles enable complete trapping up to a certain reduced rod density. The resulting triple point is independent of the trap density and attains a value $\phi_R^* \approx 1.3$. Higher densities will show only two different trapping states. While for a single particle and a static microwedge a capture is only possible for an apex angle $\alpha < 90^\circ$, an increase of the rod density leads to an increase of the maximum apex angle which allows trapping. Self-propelled rods coherently self-trap at the kink of the trap and jam. Hereby a small immobile cluster can be formed which grows and leads to a filling of the wedge. Therefore, in the studied density regime, a trapping state is possible for apex angles up to $\alpha \approx 120^\circ$. The influence of rotational noise, which may arise from fluctuations in the swimming direction as manifested by *run-and-tumble* motion of swimming bacteria, has been accounted for by adding Gaussian white noise to the equation of rotational motion Eq. (5). No significant effect on the trapping state diagram was found for typical values of the effective rotational diffusivity of bacterial swimmers [38].

B. Mobile microwedge

We now consider a moving trap. Simulation results for the trapping state diagram in the plane spanned by reduced trap velocity v/v_0 and apex angle α are shown in Fig. 4 combined with appropriate simulation snapshots characterizing the final state. As a first general finding, the state diagram has the same topology as that for a single rod if one does not

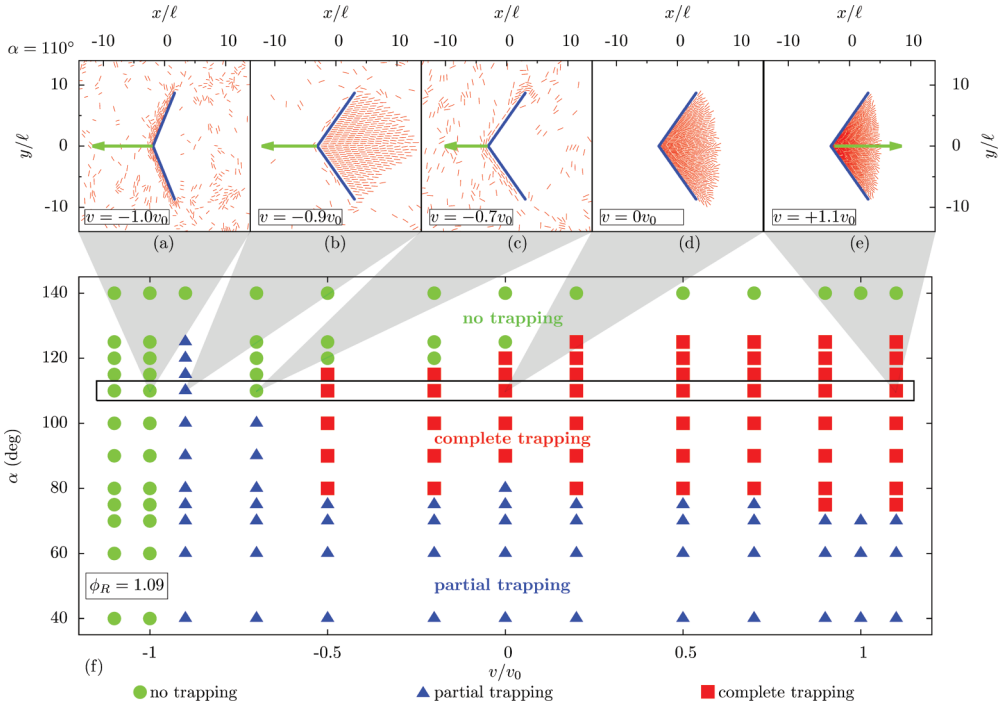

FIG. 4. (Color online) Trapping state diagram and simulation snapshots of the final state at finite rod density $\phi_R = 1.09$. [(a)–(e)] Simulation snapshots for an apex angle $\alpha = 110^\circ$. The respective dragging velocity of the trap is given in each figure and indicated by a scaled arrow. (f) State diagram showing the three different trapping states in the plane spanned by the reduced net velocity and the trap apex angle α. Circles correspond to no trapping, triangles to partial trapping, and squares to complete trapping.

discriminate between partial trapping and complete trapping. Of course, the actual numbers for the trapping to no trapping transition are significantly shifted. In particular, the worst case of trapping which occurs at an opening angle of 90° for a static microwedge [see Fig. 2(a) and Ref. [38]] is now significantly shifted towards an opening angle of about 110° at a negative reduced drag velocity of about −0.7. A corresponding snapshot of the empty microwedge is shown in Fig. 4(c).

If the trap velocity is varied at a fixed opening angle of 110°, as indicated by the different snapshots in Figs. 4(a)–4(e), there is an intermediate trapping effect at reduced negative drags close to −1, as indicated in Fig. 4(b). In this case, rods can catch up with the moving net to accumulate inside the wedge. This is opposed to strongly negative dragging velocities $v \leqslant -v_0$, where the wedge is faster than the rods on average, which leads to an accumulation of particles outside the net [see Fig. 4(a)].

Let us focus on the partial trapping situation of rods which are only slightly faster than the net as shown in Fig. 4(b). We observe a large swarm following the movement of the net. The structure of the swarm is characterized by a significant degree of nematic (or polar) order which stems from the repulsive rod interactions. The big swarm therefore is a result of rod self-assembly templated by the moving net. The net plays the role of a leader which guides the swarm. This is an interesting collective effect which can be, in principle, exploited to control and guide assemblies of active particles at will [66] or to align them dynamically in an efficient way. Qualitatively, the tendency of alignment can be seen from only a single rod [see Fig. 2(b)] which tries to orient along the drag direction. The rod interaction, however, dramatically increases the alignment, leading to a large orientated swarm.

Further increasing positive drag speed will compress the trapped particles, leading to a larger number density of the captured particles inside the net. Therefore, at higher speeds, the threshold to a no-trapping state is shifted towards larger opening angles.

We now focus on the transition line between partial trapping and complete trapping; see the squares and triangles in Fig. 4(f). At fixed opening angle (say at about 80°), this line also shows an interesting reentrance effect for increasing drag velocities as embodied in the highly nontrivial state sequence of partial trapping-complete trapping-partial trapping-complete trapping. The first transition from partial trapping to complete trapping has to do with the efficient nematization which then becomes less efficient at almost zero drag velocities. The ultimative transition to complete trapping is then an effect of rod compression inside the net for increasing drag velocities. Interestingly, starting with a resting net with opening angles slightly below 90°, the trapping efficiency increases no matter in which direction the microwedge is dragged.

We now characterize the directed self-assembled state more carefully by monitoring the area covered by the trapped particles and the actual nematic order. First, we draw a convex hull around all trapped particles which defines an area A_c. We normalize this area to the inside area $A_0 = (\ell_T/8)\sin\alpha/2$ of the wedge. Results for A_c/A_0 as a function of the drag speed are presented in Fig. 5(a) at fixed opening angle α. In line with the huge nematic wake discussed earlier, the ratio A_c/A_0 vastly exceeds unity for negative drags close to $-v_0$. In fact, A_c/A_0 has a maximum as a function of v/v_0, which points

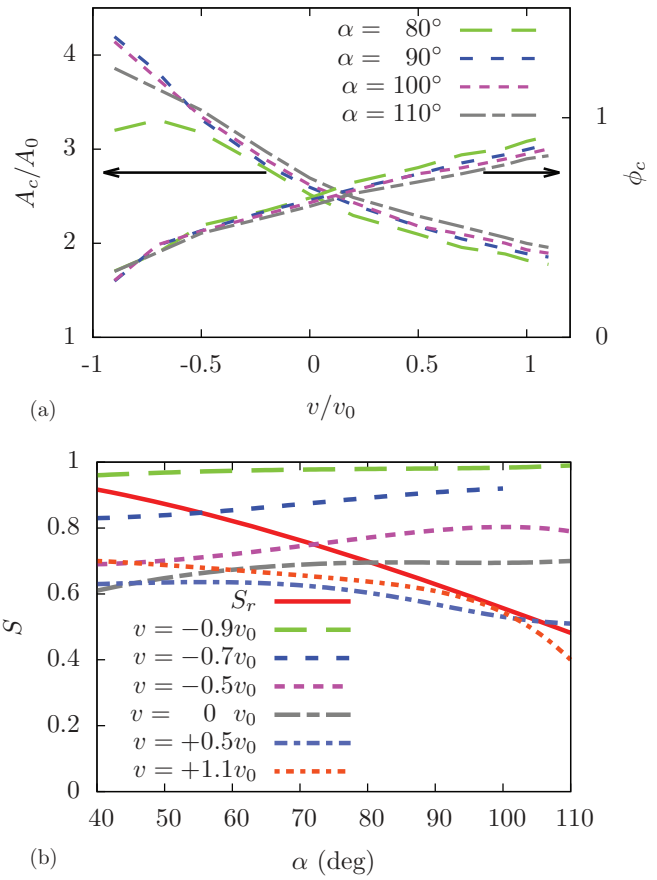

FIG. 5. (Color online) (a) Relative area occupied by captured swimmers A_c/A_0 and resulting packing fraction ϕ_c for $\phi_R = 1.09$ and varying drag velocities for four apex angles. (b) Dependence of the nematic order parameter S on the apex angle for various drag velocities (dashed lines). The reference value S_r for a perfect cone orientation of the captured rods is given by the solid line.

to a very efficient wake area that contains particles which are dragged through the liquid by the moving wedge.

Second, we analyze the degree of nematic ordering in the trapped particles by calculating the average

$$S = \langle 2\cos^2\theta_i - 1\rangle, \tag{15}$$

where θ_i is the angle between the rod orientation of the ith rod and the drag velocity. The average $\langle\ldots\rangle$ refers to an average over all captured rods for a variety of different initial configurations. The nematic order parameter S is defined as usual in two spatial dimensions. For a perfect alignment of all trapped rods, $S = 1$, while S vanishes if there is no orientational ordering at all. We relate this quantity S to a perfect cone filling of the rods where the orientational direction is antiradially towards the origin of the wedge. In this reference situation, the nematic order parameter S_r is given by

$$S_r = \frac{1}{\alpha}\int_{-\alpha/2}^{\alpha/2}(2\cos^2\theta - 1)d\theta = \sin\alpha/\alpha. \tag{16}$$

In Fig. 5(b), S is shown versus the opening angle for fixed drag speeds. The cone normalization S_r is also given. For the nematic swarm at $v/v_0 = -0.9$, S clearly exceeds S_r. This is inverted for very high positive drags $v > v_0$, where $S < S_r$

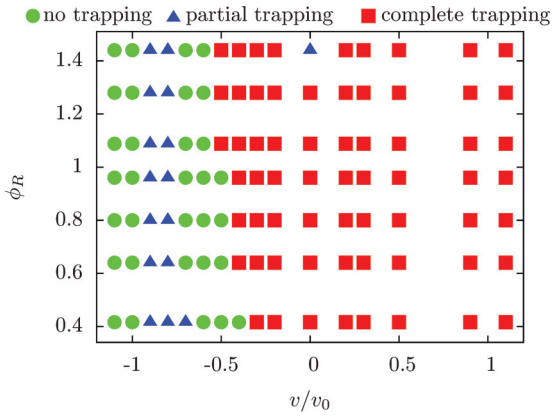

FIG. 6. (Color online) Trapping states for a fixed apex angle $\alpha = 110^\circ$.

holds over the full range of opening angles. This finding can be attributed mainly to particle misorientations at the wedge boundary close to the end of the wedge; see again the snapshot of Fig. 4(e).

In addition, we consider a system with a fixed apex angle $\alpha = 110^\circ$ and vary the reduced rod packing fraction ϕ_R and the dragging velocity. The data contained in Fig. 6 show that the dependence on the rod density is weak, providing the same state sequence as for the special rod density selected previously for Fig. 4(f). Only in the case of extreme rod densities $\phi_R > \phi_R^* = 1.3$ is the area of the net not large enough to accommodate all particles. This leads to a partial trapping state instead of complete trapping, as indicated in Fig. 6 for a static microwedge at high rod densities.

We expect our results to be robust against hydrodynamic far-field interactions, which are expected to be less important for the particle dynamics at high local particle densities, as found inside the trap, due to mutual hydrodynamic screening [67] and the small magnitude of the flows fields generated by the microswimmers [62] and the moving wedge. Moreover, the presence of no-slip trap boundaries in microfluidic devices are expected to strongly suppress hydrodynamic long-range interactions between swimmers due to cancellation effects from the hydrodynamic images [53].

V. CONCLUSIONS

While there is a considerable amount of detailed knowledge about how to trap macroscopic particles and passive particles in static traps such as colloids using optical tweezers or atoms in a Paul trap, is it much less clear how large numbers of active microscopic particles can be captured in an efficient way. Using computer simulations, we have studied a dragged chevron-shaped trap which allows us to capture several self-propelled rods in an irreversible manner. A microwedge with variable apex angle α enforces active particles to rectify their swimming direction and stimulates the formation of microscopic cluster which may subsequently act as a nucleus for a fast-growing mesoscopic aggregate of captured rods. We have demonstrated the crucial role of the apex angle and the drag velocity of the trap. A nonzero drag velocity imposes dynamic nematization and layerlike ordering of the clustered rods provided the drag velocity is slightly above $-v_0$ ($v \gtrsim -v_0$). We have highlighted the influence of collective self-trapping by comparing results for many self-propelled rods with the single-particle case. The dramatical collective response of self-propelled rods to a minor change in the boundary shape or drag velocity is remarkable and remains unseen for passive systems exposed to external boundaries or electromagnetic traps.

Collective trapping of ensembles of active particles in moving traps can be verified by experiments using rod-shaped bacteria [68] or driven polar granular rods [69] exposed to geometrically structured boundaries [23,54,55]. While the presented results are valid for linearly propagating swimmers, it would be interesting to study a trapping device for several swimmers moving on circlelike pathways [28,70–72]. Furthermore, it would be interesting to exploit the trapping scenarios proposed here to design a trapping device which is capable of extracting swimmers with a specific velocity bandwidth from a mixture of active particles with a strong spread in motility. According to the results in Fig. 4, such velocity-selective trapping could be envisaged by dragging the net at a judiciously chosen negative drag velocity such as to facilitate templated clustering of a subset of swimmers whose individual motility closely resembles that of the moving net.

An interesting open question is in regard to what extent the details of the propulsion mechanism affect the self-trapping behavior of the rods. In particular, it would be interesting to study whether puller- and pusher-type swimmers exhibit different trapping behaviors. These problems will necessitate the use of more sophisticated simulation schemes [73–75] and bring us also to the question regarding the importance of hydrodynamic near-field interactions [76], which are ignored in our model. Real bacteria are usually propelled by flagella attached to the bacterial body whose internal configuration will presumably change at high bacterial density, under strong confinement or at an obstacle [77]. These flagellar interactions may lead to more specific effects which are neglected in our model but could be included on a coarse-grained level in future studies. In particular, one could introduce a density-dependent microscopic mobility which is known to have a considerable effect on the collective behavior in bulk [78]. Finally, it would be interesting to model the properties of the trapped polar state of rods using continuum elasticity theory following recent efforts in this direction for the wetting behavior of (passive) liquid crystals confined in wedges [79–81].

ACKNOWLEDGMENTS

We thank J. Tailleur for helpful discussions. This work was financially supported by the ERC Advanced Grant INTERCOCOS (Grant No. 267499) and by the DFG within SFB TR6 (Project No. D3).

[1] W. Radcliffe, *Fishing from the Earliest Times* (John Murray, London, 1926).
[2] M. E. Cates, Rep. Prog. Phys. **75**, 042601 (2012).
[3] P. Romanczuk, M. Bär, W. Ebeling, B. Linder, and L. Schimansky-Geier, Europhys. Lett. Spec. Top. **202**, 1 (2012).

[4] M. C. Marchetti, J. F. Joanny, S. Ramaswamy, T. B. Liverpool, J. Prost, M. Rao, and R. A. Simha, Rev. Mod. Phys. **85**, 1143 (2013).
[5] T. Vicsek and A. Zafeiris, Phys. Rep. **517**, 71 (2012).
[6] C. Dombrowski, L. Cisneros, S. Chatkaew, R. E. Goldstein, and J. O. Kessler, Phys. Rev. Lett. **93**, 098103 (2004).
[7] A. Sokolov, I. S. Aranson, J. O. Kessler, and R. E. Goldstein, Phys. Rev. Lett. **98**, 158102 (2007).
[8] X. Chen, X. Dong, A. Be'er, H. L. Swinney, and H. P. Zhang, Phys. Rev. Lett. **108**, 148101 (2012).
[9] F. G. Woodhouse and R. E. Goldstein, Phys. Rev. Lett. **109**, 168105 (2012).
[10] J. Schwarz-Linek, C. Valeriani, A. Cacciuto, M. E. Cates, D. Marenduzzo, A. N. Morozov, and W. C. K. Poon, Proc. Natl. Acad. Sci. USA **109**, 4052 (2012).
[11] W. R. DiLuzio, L. Turner, M. Mayer, P. Garstecki, D. B. Weibel, H. C. Berg, and G. M. Whitesides, Nature **435**, 1271 (2005).
[12] E. Lauga, W. R. DiLuzio, G. M. Whitesides, and H. A. Stone, Biophys. J. **90**, 400 (2006).
[13] J. Hill, O. Kalkanci, J. L. McMurry, and H. Koser, Phys. Rev. Lett. **98**, 068101 (2007).
[14] V. B. Shenoy, D. T. Tambe, A. Prasad, and J. A. Theriot, Proc. Natl. Acad. Sci. USA **104**, 8229 (2007).
[15] S. Schmidt, J. van der Gucht, P. M. Biesheuvel, R. Weinkamer, E. Helfer, and A. Frey, Europ. Biophys. J. **37**, 1361 (2008).
[16] X. Garcia, S. Rafaï, and P. Peyla, Phys. Rev. Lett. **110**, 138106 (2013).
[17] R. Golestanian, T. B. Liverpool, and A. Ajdari, Phys. Rev. Lett. **94**, 220801 (2005).
[18] A. Erbe, M. Zientara, L. Baraban, C. Kreidler, and P. Leiderer, J. Phys.: Condens. Matter **20**, 404215 (2008).
[19] J. Palacci, C. Cottin-Bizonne, C. Ybert, and L. Bocquet, Phys. Rev. Lett. **105**, 088304 (2010).
[20] R. Dreyfus, J. Baudry, M. L. Roper, M. Fermigier, H. A. Stone, and J. Bibette, Nature **437**, 862 (2005).
[21] P. Tierno, R. Golestanian, I. Pagonabarraga, and F. F. Sagues, J. Phys. Chem. B **112**, 16525 (2008).
[22] B. Kaehr and J. B. Shear, Lab Chip **9**, 2632 (2009).
[23] G. Volpe, I. Buttinoni, D. Vogt, H. J. Kümmerer, and C. Bechinger, Soft Matter **7**, 8810 (2011).
[24] A. Snezhko, M. Belkin, I. S. Aranson, and W.-K. Kwok, Phys. Rev. Lett. **102**, 118103 (2009).
[25] A. Snezhko and I. S. Aranson, Nat. Mat. **10**, 698 (2011).
[26] G. Rückner and R. Kapral, Phys. Rev. Lett. **98**, 150603 (2007).
[27] T. Ohta and T. Ohkuma, Phys. Rev. Lett. **102**, 154101 (2009).
[28] F. Kümmel, B. ten Hagen, R. Wittkowski, I. Buttinoni, R. Eichhorn, G. Volpe, H. Löwen, and C. Bechinger, Phys. Rev. Lett. **110**, 198302 (2013).
[29] A. Reinmüller, H. J. Schöpe, and T. Palberg, Langmuir **29**, 1738 (2013).
[30] J. Palacci, S. Sacanna, A. P. Steinberg, D. J. Pine, and P. M. Chaikin, Science **339**, 936 (2013).
[31] O. Raz and A. M. Leshansky, Phys. Rev. E **77**, 055305 (2008).
[32] W. Gao, D. Kagan, O. S. Pak, C. Clawson, S. Campuzano, E. Chuluun-Erdene, E. Shipton, E. E. Fullerton, L. Zhang, E. Lauga *et al.*, Small **8**, 460 (2011).
[33] L. Baraban, M. Tasinkevych, M. N. Popescu, S. Sanchez, S. Dietrich, and O. G. Schmidt, Soft Matter **8**, 48 (2012).
[34] M. N. Popescu, M. Tasinkevych, and S. Dietrich, Europhys. Lett. **95**, 28004 (2011).
[35] L. Angelani and R. D. Leonardo, New J. Phys. **12**, 113017 (2010).
[36] E. C. Redmond and C. J. Griffith, J. Food Protect. **66**, 130 (2003).
[37] J. Taylor, K. Lai, M. Davies, D. Clifton, I. Ridley, and P. Biddulph, Environ. Int. **37**, 1019 (2011).
[38] A. Kaiser, H. H. Wensink, and H. Löwen, Phys. Rev. Lett. **108**, 268307 (2012).
[39] H. H. Wensink and H. Löwen, Phys. Rev. E **78**, 031409 (2008).
[40] B. ten Hagen, R. Wittkowski, and H. Löwen, Phys. Rev. E **84**, 031105 (2011).
[41] M. Grzelczak, J. Vermant, E. M. Furst, and L. M. Liz-Marzän, ACS Nano **4**, 3591 (2010).
[42] P. Galajda, J. Keymer, P. Chaikin, and R. Austin, J. Bacteriol. **189**, 8704 (2007).
[43] V. Kantsler, J. Dunkel, M. Polin, and R. E. Goldstein, Proc. Natl. Acad. Sci. USA **110**, 1187 (2013).
[44] J. Tailleur and M. E. Cates, Europhys. Lett. **86**, 60002 (2009).
[45] M. B. Wan, C. J. Olson Reichhardt, Z. Nussinov, and C. Reichhardt, Phys. Rev. Lett. **101**, 018102 (2008).
[46] J. A. Drocco, C. J. Olson Reichhardt, and C. Reichhardt, Phys. Rev. E **85**, 056102 (2012).
[47] M.-B. Wan and Y. Jho, Soft Matter **9**, 3255 (2013).
[48] P. K. Ghosh, V. R. Misko, F. Marchesoni, and F. Nori, Phys. Rev. Lett. **110**, 268301 (2013).
[49] R. DiLeonardo, L. Angelani, D. DellArciprete, G. Ruocco, V. Iebba, S. Schippa, M. P. Conte, F. Mecarini, F. D. Angelis, and E. D. Fabrizio, Proc. Natl. Acad. Sci. USA **107**, 9541 (2010).
[50] A. Sokolov, M. M. Apodaca, B. A. Grzyboski, and I. S. Aranson, Proc. Natl. Acad. Sci. USA **107**, 969 (2010).
[51] I. S. Aranson and L. S. Tsimring, Rev. Mod. Phys. **78**, 641 (2006).
[52] S. Ramaswamy, Annu. Rev. Condens. Matter Phys. **1**, 323 (2009).
[53] H. H. Wensink, J. Dunkel, S. Heidenreich, K. Drescher, R. E. Goldstein, H. Löwen, and J. M. Yeomans, Proc. Natl. Acad. Sci. USA **109**, 14308 (2012).
[54] D. L. Englert, M. D. Manson, and A. Jayaraman, Nat. Protocols **5**, 864 (2010).
[55] G. Miño, T. E. Mallouk, T. Darnige, M. Hoyos, J. Dauchet, J. Dunstan, R. Soto, Y. Wang, A. Rousselet, and E. Clement, Phys. Rev. Lett. **106**, 048102 (2011).
[56] G. V. Kolmakov, A. Schaefer, I. Aranson, and A. C. Balazs, Soft Matter **8**, 180 (2012).
[57] V. Blickle, J. Mehl, and C. Bechinger, Phys. Rev. E **79**, 060104(R) (2009).
[58] H. H. Wensink and H. Löwen, J. Phys.: Condens. Matter **24**, 464130 (2012).
[59] T. Kirchhoff, H. Löwen, and R. Klein, Phys. Rev. E **53**, 5011 (1996).
[60] H. Graf and H. Löwen, Phys. Rev. E **59**, 1932 (1999).
[61] M. M. Tirado, C. L. Martinez, and J. G. de la Torre, J. Chem. Phys. **81**, 2047 (1984).
[62] K. Drescher, J. Dunkel, L. H. Cisneros, S. Ganguly, and R. E. Goldstein, Proc. Natl. Acad. Sci. USA **108**, 10940 (2011).
[63] H. Löwen and G. P. Hoffmann, Phys. Rev. E **60**, 3009 (1999).
[64] V. Narayan, S. Ramaswamy, and N. Menon, Science **317**, 105 (2007).
[65] See Supplemental Material at http://link.aps.org/supplemental/10.1103/PhysRevE.88.022311 for movies showing the occurring trapping mechanisms for the single-particle case.

[66] R. Ledesma-Aguilar, H. Löwen, and J. M. Yeomans, Eur. Phys. J. E **35**, 9746 (2012).
[67] E. S. Muthukumar, Macromolecules **16**, 1475 (1983).
[68] L. H. Cisneros, R. Cortez, C. Dombrowski, R. E. Goldstein, and J. O. Kessler, Exp. Fluids **43**, 737 (2007).
[69] D. Volfson, A. Kudrolli, and L. S. Tsimring, Phys. Rev. E **70**, 051312 (2004).
[70] A. Kaiser and H. Löwen, Phys. Rev. E **87**, 032712 (2013).
[71] S. van Teeffelen, U. Zimmermann, and H. Löwen, Soft Matter **5**, 4510 (2009).
[72] M. Mijalkov and G. Volpe, Soft Matter **9**, 6376 (2013).
[73] T. Ishikawa and T. J. Pedley, Phys. Rev. Lett. **100**, 088103 (2008).
[74] M. T. Downton and H. Stark, J. Phys.: Condens. Matter **20**, 204101 (2009).
[75] I. O. Götze and G. Gompper, Phys. Rev. E **82**, 041921 (2010).
[76] J. K. G. Dhont, *An Introduction to the Dynamics of Colloids* (Elsevier, Amsterdam, 1996).
[77] L. Cisneros, C. Dombrowski, R. E. Goldstein, and J. O. Kessler, Phys. Rev. E **73**, 030901 (2006).
[78] F. D. C. Farrell, M. C. Marchetti, D. Marenduzzo, and J. Tailleur, Phys. Rev. Lett. **108**, 248101 (2012).
[79] O. J. Dammone, I. Zacharoudiou, R. P. A. Dullens, J. M. Yeomans, M. P. Lettinga, and D. G. A. L. Aarts, Phys. Rev. Lett. **109**, 108303 (2012).
[80] N. M. Silvestre, Z. Eskandari, P. Patrício, J. M. Romero-Enrique, and M. M. Telo da Gama, Phys. Rev. E **86**, 011703 (2012).
[81] A. O. Parry, C. Rascón, E. A. G. Jamie, and D. G. A. L. Aarts, Phys. Rev. Lett. **108**, 246101 (2012).